J. Fluid Mech. (1982), *vol.* 114, *pp.* 501–528
Printed in Great Britain

Interaction of free-stream turbulence with screens and grids: a balance between turbulence scales

By J. TAN-ATICHAT, H. M. NAGIB

Department of Mechanics and Mechanical Aerospace Engineering, Illinois Institute of Technology, Chicago

AND R. I. LOEHRKE

Department of Mechanical Engineering, Colorado State University, Fort Collins

(Received 13 November 1978 and in revised form 19 January 1981)

Effects of screens and perforated plates (grids) on free-stream turbulence are studied in several test flow conditions. The level, structure and decay of the turbulence generated by such 'manipulators' depend in part on their shear-layer instabilities, and can therefore be modified by inserting additional devices immediately downstream. The performance of screens and some perforated plates is found to depend on the characteristics of the incoming flow such as velocity, turbulence level and spectra. Combinations of perforated plates and screens are found to be very effective flow manipulators. By optimizing the intermanipulator separation and carefully matching the scales between the manipulator pair, the turbulence decay rate downstream of a grid can be quadrupled.

1. Introduction

It is essential in many practical applications to tailor the properties of a fluid stream to fit a specific need. For example the success of experiments on the transition to turbulence depends on free-stream flows with uniform mean velocity and low turbulence. On the other hand, many industrial and chemical processes require highly turbulent flows to enhance mixing. This paper focuses on the problem of turbulence reduction in streams with uniform mean velocity. A broader picture of the management and control of free-stream turbulence has been discussed in other publications, e.g. Loehrke & Nagib (1972, 1976) and Wigeland, Ahmed & Nagib (1978).

Traditionally, screens, grids or perforated plates, honeycombs, and other flow inserts, hereafter referred to as flow or turbulence manipulators (since they act on both the mean and fluctuating components of velocity), were utilized to reduce turbulence, to suppress swirls, and to eliminate or reduce mean velocity non-uniformities. The present study represents part of a larger effort aimed at uncovering mechanisms which control the operation of these manipulators; for example see Loehrke & Nagib (1972, 1976), Nagib, Way & Tan-atichat (1975), Tan-atichat, Nagib & Loehrke (1972) and Wigeland *et al.* (1978). Experiments dealing with screens and perforated plates (grids) operating individually and in combination are described following a brief review of the pertinent literature.

Much of the considerable store of theoretical and experimental information on the

effect of screens on turbulence can be found in the reviews by Corrsin (1963) and by Laws & Livesey (1978), and in the classical texts of Batchelor (1953), Townsend (1976) and Hinze (1975). Lattices of parallel or crossed cylinders (and more recently plates with circular or rectangular perforations) have been used to generate free-stream turbulence as well as to suppress it. Whether one views these devices as reducers or producers of turbulence depends on the Reynolds number at which the device is operated, the turbulence properties of the stream in absence of the device, the properties of the turbulence created by the device and the downstream decay time provided.

All existing theories of turbulence suppression bypass the details of the rise and fall in the velocity fluctuations that occur immediately downstream of a screen operating at above-critical conditions. Instead, the screen is usually characterized by a loss coefficient $\Delta P/\frac{1}{2}\rho U_\infty^2$, referred to as the pressure-drop coefficient K. A second empirical quantity, the mean velocity refraction coefficient α, is also used to characterize a screen. The reduction of turbulence level in a stream due to passage through a screen has been estimated by Batchelor (1945) and Taylor & Batchelor (1949) in terms of these related parameters for low-level incident turbulence (see e.g. Dryden & Schubauer 1949; Laws & Livesey 1978). Although these estimates are in qualitative agreement with experiment, considerable scatter in the experimental data exists. In spite of the fact that these theories do not account for turbulence generation by the screen, the data for supercritical screen operation are found to be in better agreement with theory than those for subcritical operation (e.g. see Schubauer, Spangenberg & Klebanoff 1950).

It appears that the details of the generated turbulence, viz. level, structure and scale, should influence the performance of the screen. Corrsin (1963) has suggested that the effectiveness of turbulence-reducing, supercritical screens may be enhanced if the screen turbulence is of somewhat smaller structure than the turbulence to be eliminated. The properly matched 'additional large-wavenumber energy may be expected to accelerate the spectral transfer rate of the pre-existing small-wavenumber energy, thus increasing its decay rate'.

For grid-generated turbulence it has been established experimentally by Comte-Bellot & Corrsin (1966) that over a wide range of Reynolds numbers and for different grid geometries the turbulence energy decays downstream of a grid according to the relation

$$\left[\frac{U_\infty}{u'}\right]^2 = \frac{b}{C_D}\left[\frac{x}{M} - \frac{x_0}{M}\right]^m, \tag{1}$$

with m ranging from approximately 1·2 to 1·3. However, this 'law' of the initial period of decay does not apply to the first 20 to 30 mesh lengths downstream of the grid, where transverse inhomogeneities are usually present. The constant x_0, which is used to account in part for this inhomogeneity, designates the position of a virtual origin and is usually found to be in the range from $2M$ to $15M$ for square-mesh grids. The value of b or b/C_D appears to depend on the shape of the grid and, hence, the shape of the emerging velocity profiles. Typical values of b/C_D (or A_1) in Comte-Bellot & Corrsin (1966) range from below 6 for disk grids to 20 or higher for biplane grids. Other values for b (with $m = 1{\cdot}0$) reported by Batchelor (1953) are: 101 for a double row of rods, 53 for a single row of rods and 91 for a single row of slats. How-

ever, the studies of Tsuji (1955, 1956) point out that the turbulence downstream of a grid will depend on the upstream turbulence. Batchelor (1953) also remarks that the early measurements of the decay of grid-generated turbulence were 'a little confused by the existence in the wind-tunnel stream of turbulence from sources other than the grid'. Based on these findings one may surmise that the dependence on the upstream flow conditions must be introduced into (1) if it is applied to grids in flows with considerable turbulence levels. Such dependence should be more evident in the case of screens, owing to their lower Reynolds numbers. As a result, the quoted turbulence-reduction factor of any given screen must reflect such dependence. To date, no known experiments or theory have focused on this subject.

An additional phenomenon, which may influence the effectiveness of turbulence-reducing screens or grids, is the emergence of large-scale instability associated with high-solidity devices. Corrsin (1944) and others have observed a bi-stable coalescing of the jets issuing from some grids having a solidity greater than about 0·42. This phenomenon has the effect of introducing persistent mean velocity variations into the flow and of greatly reducing the decay rate of the newly formed turbulence, e.g. see Loehrke & Nagib (1972) and Klebanoff & Tidstrom (1959).

The general purpose of the present experiments was to show that the properties of both the incoming and the newly formed (i.e. manipulator-generated) turbulence are important factors affecting the performance of grids and screens which are normally employed for turbulence reduction. Also, in light of the experiments performed with honeycomb manipulators by Loehrke & Nagib (1976), it was of interest to see what role, if any, shear-layer instabilities played in the production of new turbulence downstream of grids and to determine whether these instabilities would be modified by using coupled manipulators.

2. Facilities, instrumentation and test-flow conditions

The data presented in this paper were obtained in two wind tunnels: the small (7·2 cm diameter test section), compressed-air-driven wind tunnel described in detail by Loehrke & Nagib (1972) and a larger (15·2 cm diameter test section), blower-driven wind tunnel. A complete description of the larger wind tunnel is given by Ahmed, Wigeland & Nagib (1976).

Standard hot-wire instrumentation was used for mean, r.m.s. and spectral measurements of the streamwise flow velocity. For turbulence-intensity measurements it is estimated that the electronic noise from the instrumentation and experimental uncertainty is equivalent to approximately 0·18 % turbulence intensity. In turbulence spectral measurements the frequency uncertainty is $\pm 5{\cdot}5$ Hz at 20 Hz and increases to ± 21 Hz at 3 kHz. The accuracy of the output of the spectrum analyser is typically 5 %. An output of 1 V corresponds to a velocity of 3·05 m/s (10 ft/s). The bandwidth of the spectra in figures 3 and 11 is 10 Hz and in figure 4 the bandwidth is 50 Hz. Further details are given by Loehrke & Nagib (1972, 1976).

Table 1 summarizes some of the important physical characteristics of the flow manipulators used. In addition, the pressure-drop coefficient K $(=\Delta P/\frac{1}{2}\rho U_\infty^2)$, the mesh Reynolds number $R_M = U_\infty M/\nu$ and the Reynolds number R_d based on the wire diameter of the screens, are tabulated for $U_\infty = 4{\cdot}6$ m/s (15 ft/s). Three types of perforated plates are used, and are referred to as PP1, PP2, and PP3. All the

Screens	Wire diameter [mm] and material	Mesh [cm]	σ	K†	l_M [cm]	R_M† and (R_d)†
0	0·13 Dacron	0·084	0·28	0·86	0·013	245 (40)
3	0·28 Aluminium	0·16	0·32	0·80	0·028	460 (85)
5	0·64 Stainless steel	0·25	0·36	1·12	0·064	735 (190)
6	0·18 Stainless steel	0·091	0·35	1·02	0·018	260 (55)
Perforated plates (1·6 mm thick sheet steel)	Hole diameter [mm]					
PP1	1·59	0·28	0·70	7·9	0·16	800
PP2	3·56	0·48	0·49	2·0	0·16	1380
PP3	6·35	0·80	0·42	1·5	0·16	2300

† At $U_\infty = 4{\cdot}6$ m/s.

TABLE 1. Characteristics of screens and perforated plates.

plates are standard stock, punched steel plates 1·6 mm thick, with circular holes arranged in a hexagonal array. Because of the manner in which the plates are manufactured, one edge of the hole is sharp while the other is slightly rounded. In spite of this, no influence of the plate orientation with respect to the flow direction could be detected. The geometrical characteristics of the three plates are tabulated in the bottom section of table 1. All of the plates and screens spanned the entire test section of the wind tunnel in which they were tested. Combined turbulence manipulators consisted of a single screen placed downstream of a perforated plate with the separation distance between the two (Δx) ranging from 0 (i.e. no separation) to 3·49 cm. The combinations are treated as coupled turbulence manipulators in the same manner as discussed by Tan-atichat *et al.* (1972) and Loehrke & Nagib (1972, 1976).

Tsuji (1955, 1956) has shown that the level and structure of turbulence in the flow upstream of a grid can have a pronounced effect on the decay of turbulence downstream from the grid. In many applications where such devices are used for turbulence control the structure of the incoming flow may be largely unknown. At any rate, the structure will vary from one application to another. For these reasons several different test-flow conditions were generated for this investigation and some care was taken in documenting them. Four test-flow conditions, namely A, B, B' and C, were used for tests conducted in the small wind tunnel and four others, E, E', H and $H1$, were employed in the large wind tunnel. Conditions E and H in the present investigation are different from those cited by Loehrke & Nagib (1972) and Nagib *et al.* (1975). In order to produce these different flows, a turbulence generator was placed near the entrance of the test section. Figure 1 is a schematic summary of the test-flow conditions employed in this investigation. Figure 2 documents the streamwise turbulence intensity for all the test-flow conditions starting from the downstream side of the turbulence generator in each of the flow conditions. To determine the level of incoming turbulence to the manipulator being tested, refer to table 2 and note the value of S_0, then locate it on figure 2 for the appropriate test-

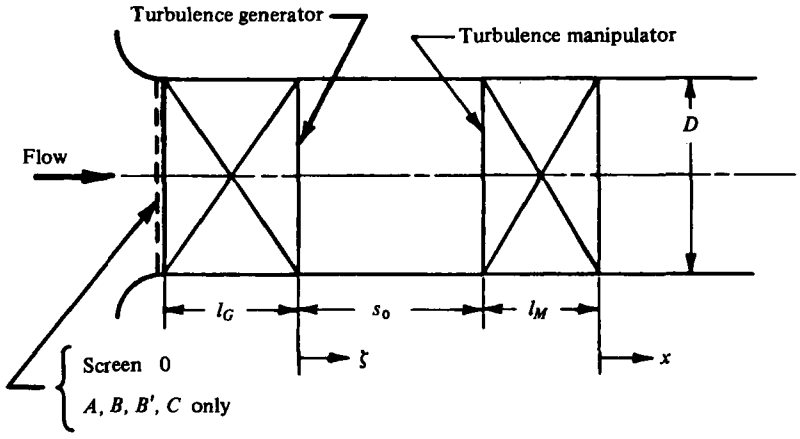

FIGURE 1. Schematic of test section for generation of test-flow conditions. l_M is the turbulence-manipulator length, described in table 1.

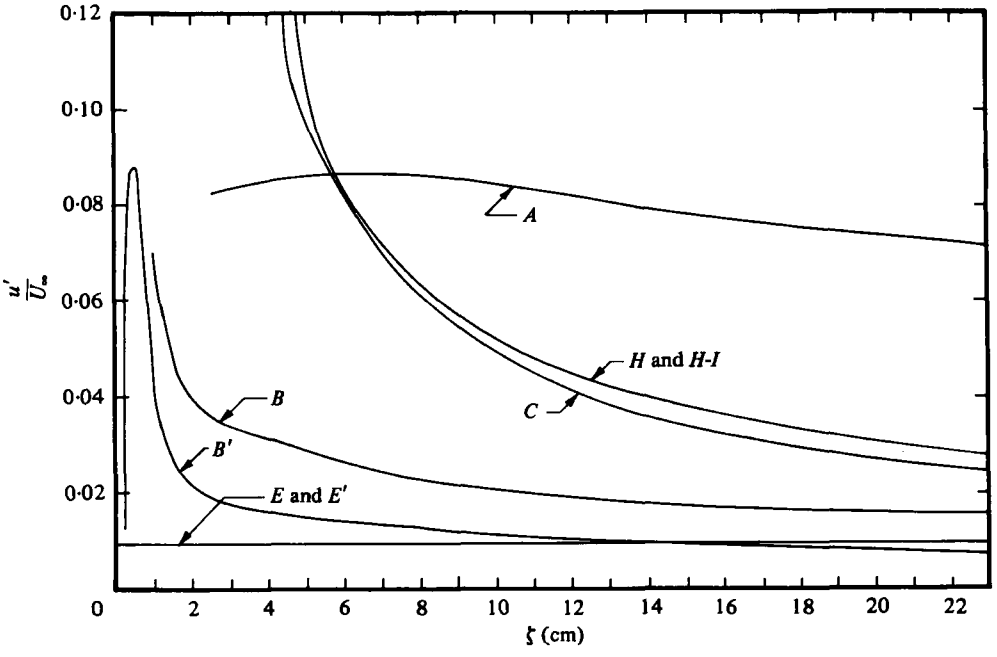

FIGURE 2. Streamwise development of turbulence intensity for various test-flow conditions. For A, B, B' and C, U_∞ = 4·6 m/s; for E, H and $H1$, U_∞ = 12·2 m/s.

flow condition. For test-flow conditions B, B', E and $H1$, u'/U_∞ must be extrapolated by the reader. However, in these cases $|\partial(u'/U_\infty)/\partial\zeta|$ is small enough to enable accurate extrapolations.

In the following description of test-flow conditions, reference to the level of turbulence intensity is aimed at describing conditions typically found in wind-tunnel settling chambers ahead of the contraction rather than in the test section. Therefore turbulence intensities of 1 to 2 % are considered 'low-turbulence' conditions.

Flow condition	Turbulence generator	Dimensions (cm) D	l_G	S_0
A	None	7·2	0	15·2
B, B'	2·5 cm straws, which are 10·2 cm downstream, followed immediately by another screen, 0	7·2	12·7	29·2
C	7·6 cm straws, 3·8 cm downstream, followed immediately by another screen, 0; and PP3, 11·4 cm further downstream	7·2	22·9	6·0
E	None (conditions were those of the settling	15·2	0	30·5
E'	chamber exit (see Ahmed *et al.* 1976))	15·2	0	0
H	PP3	15·2	0·16	12·7
$H1$	PP3	15·2	0·16	30·5

TABLE 2

Flow condition A: uniform mean velocity, moderately high turbulence intensity and minimum control of upstream history

This test-flow condition is the one which existed in the circular duct of the small wind tunnel at a moderate distance downstream of the test-section entrance screen. The turbulence manipulator to be investigated was located in the test section with its upstream end at $S_0 = 15{\cdot}2$ cm downstream from this screen, as shown in figure 1. In condition A, the plenum chamber, the bellmouth entrance to the test section and the screen located upstream of the turbulence manipulator represent the uncontrolled input parameters to the flow; in particular, to the turbulence. Therefore results obtained in this test-flow condition should be interpreted with care. A plot of the axial distribution of u'/U_∞ downstream from the test-section entrance screen is shown in figure 2. Spectral analysis of the velocity fluctuations in this test condition is summarized in figure 3. Figure 3(a) shows the spectrum to 2000 Hz while figure 3(b) provides a better resolution for the lower frequencies.

Flow conditions B, B', E and E': uniform mean velocity and uniform low turbulence intensity

In test-flow conditions B and B', a honeycomb-like matrix of 2·5 cm long straws with a screen located at its downstream end (Loehrke & Nagib 1972, 1976) was placed in the duct as described in table 2. A distance of 29·2 cm was allowed for the flow to reach near-equilibrium and for u'/U_∞ to reach a low level. The value of u'/U_∞ was 0·015 for flow condition B and 0·007 for condition B' at $U_\infty = 4{\cdot}6$ m/s. The difference between conditions B and B' was due to the incoming turbulence level and structure. Improvements made to the plenum chamber of the small wind tunnel contributed to the change from flow condition B to flow condition B'. The axial distribution of u'/U_∞ downstream of the flow condition generators is shown in figure 2. Spectral analysis of flow condition B is shown in figure 3(a). The turbulence manipulator to be examined was located in the test section with its upstream side 29·2 cm downstream from the honeycomb and screen which generated this flow condition. Both $\bar{U}$ and u' for B and B' were found to be uniform across the test section except in the thin boundary layer of the duct.

Test-flow conditions E and E' were generated in the large wind tunnel used by

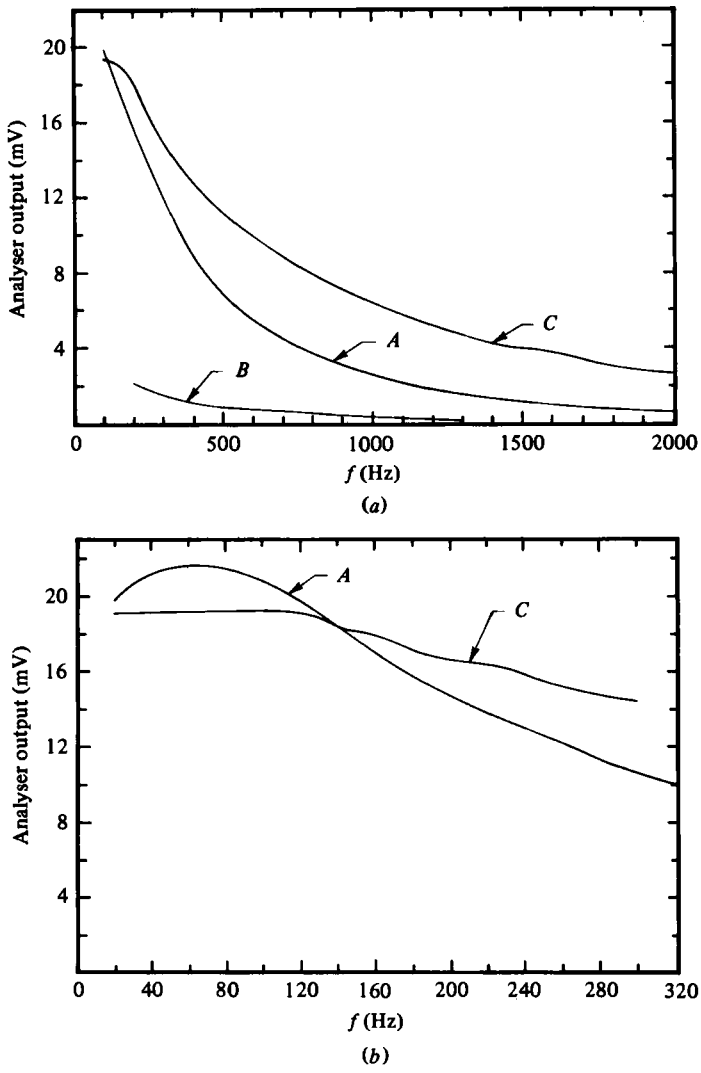

FIGURE 3. (*a*) Spectra of u for test-flow conditions A, B and C. (*b*) Low-frequency spectra for test conditions A and C.

Test-flow condition	ζ (cm)	U (m/s)	u' (mV)
A	15·2	4·7	115
B	25·4	5·3	24
C	5·1	4·6	147

Wigeland *et al.* (1978). No turbulence generators were used in the test section for these test-flow conditions. The free-stream conditions at the entrance to the test section were those of the settling chamber after passing through the 25:1 contraction section. The turbulence intensity for test-flow conditions E and E' is shown on figure 2. The only difference between test conditions E and E' was the positioning of the turbulence manipulator being tested. For flow condition E' the manipulator under test was placed at the exit of the contraction section, whereas for condition

E the manipulator was located 30·5 cm downstream of the contraction section in the constant-diameter duct.

Flow condition C: uniform mean velocity, uniform moderately high turbulence intensity and controlled upstream history

This test-flow condition was incorporated in the investigation when some of the results obtained in test-flow condition A were suspected of being influenced by the possible existence of secondary flows or swirls in the test section. This flow condition was designed to eliminate any secondary flows and to generate a uniform turbulence intensity of the same level as test condition A. As shown in figure 1, a 7·6 cm long honeycomb made of plastic straws with a screen attached to its downstream end was placed in the test section. The honeycomb was designed to break up any large-scale eddies or swirls that may have penetrated the screen at the entrance of the test section; for further discussion, see Wigeland *et al.* (1978). A perforated plate (PP3) was placed 11·4 cm downstream of the honeycomb to generate a moderately high and spatially uniform turbulence intensity. The turbulence manipulator examined in this flow condition was located with its upstream end 6·0 cm downstream of the perforated plate. With $U_\infty = 4{\cdot}6$ m/s the turbulence intensity level was approximately 0·08 at the entrance to the turbulence manipulator (see figure 2). The radial distribution of both $\overline{U}$ and u'/U_∞ at this axial location was found to be uniform (e.g. see figures 37 and 38 of Loehrke & Nagib 1972). The spectra of the axial component of the turbulence are shown in figure 3. Note that test condition C has higher energy content than flow condition A for most frequencies except those below about 140 Hz. A noted difference in the character of u' for this flow condition in comparison to condition A is the existence of a larger gradient of u'/U_∞ in the streamwise direction, i.e.

$$\left|\frac{\partial(u'/U_\infty)}{\partial\zeta}\right|_{\text{condition } C} > \left|\frac{\partial(u'/U_\infty)}{\partial\zeta}\right|_{\text{condition } A}. \tag{2}$$

Unfortunately this could not be avoided because of the need to match the level of u'/U_∞ for both test-flow conditions.

Flow conditions H and H1: uniform mean velocity, uniform moderately low turbulence intensity and partially controlled upstream history

These two test-flow conditions were generated in the larger wind tunnel. A perforated plate (PP3) was placed at the entrance to the test section to generate turbulence. Although test-flow conditions H and $H1$ have very similar turbulence intensity profiles to that of flow condition C, the criterion for classifying them as moderately low-level turbulence conditions was the streamwise positioning of the manipulators being tested. Turbulence intensity at the entrance to the manipulator being tested was about 0·043 for flow condition H and less than 0·03 for test flow $H1$.

3. Results

The results are presented in the following sequence. Firstly, the performance of single screens in different test-flow conditions is documented. Next, results obtained from perforated plates are presented. Finally, perforated-plate/screen combinations

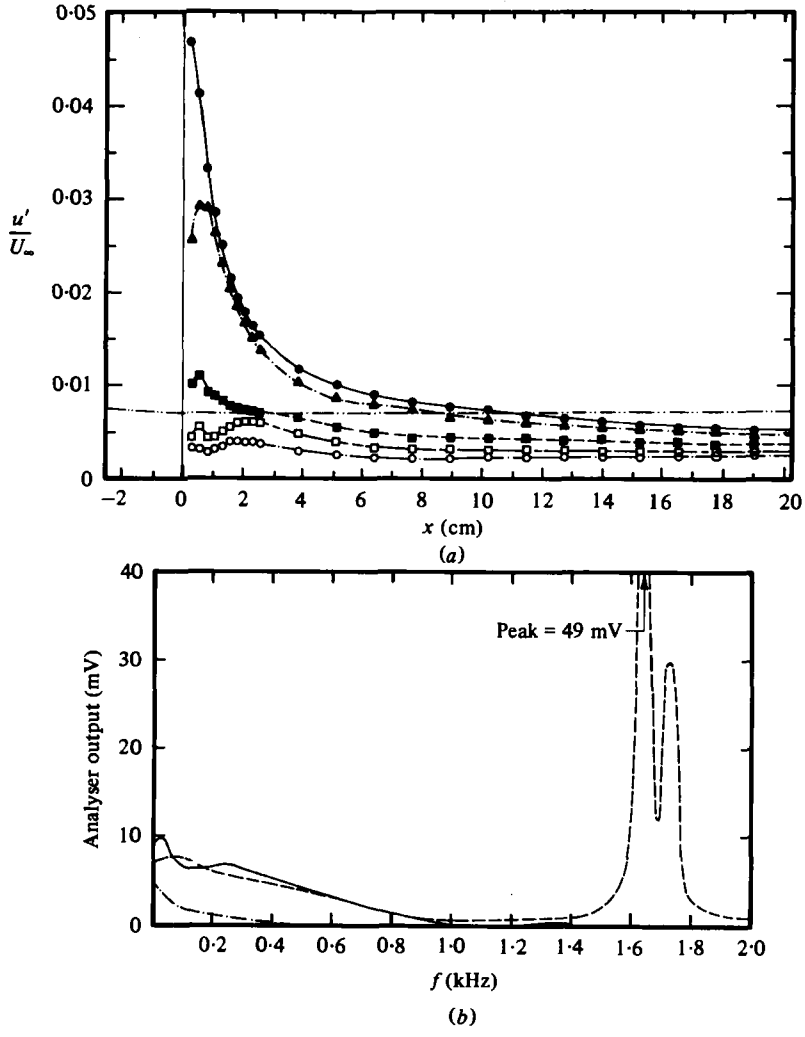

FIGURE 4. (*a*) Turbulence intensity downstream of screen 0 in test-flow condition B' as a function of free-stream velocity U_∞: ● U_∞ = 6·10 m/s, ▲ 5·33 m/s, ■ 4·57 m/s, □ 3·81 m/s, ○ 3·05 m/s. —··—·· turbulence intensity of free stream for test condition B'. (*b*) Spectra of u downstream of screen 0 in test condition B', showing instability peaks.

	U (m/s)	u' (mV)	x (cm)
·—·—	3·0	6·4	0·13
——	4·6	29·5	0·64
— — —	5·5	73	0·25

are examined. The data consist primarily of plots of turbulence intensities and turbulence decay. From the results of Comte-Bellot & Corrsin (1966) it should be evident that plots of the energy decay rate (i.e. the slopes of the decay curves) shown in the present paper will not remain constant over a wide range of downstream distances, i.e. decay times. These turbulence-decay data are plotted only as a guide to show how the turbulence energy varies with downstream distance for the different cases. Mean velocity $\bar{U}$ profiles and spectra of u are shown whenever these provide

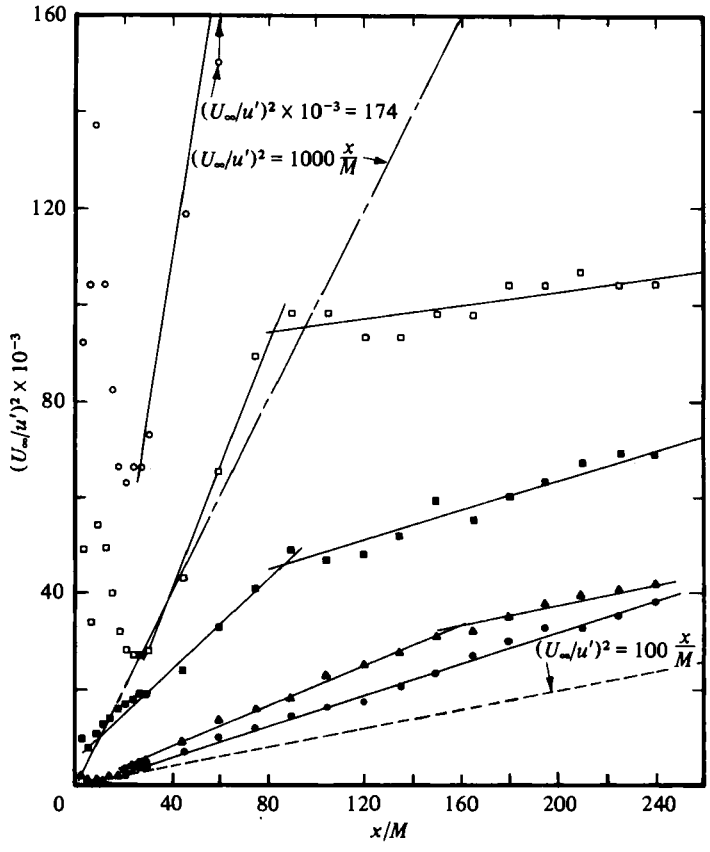

FIGURE 5. Turbulence decay downstream of screen 0 in test condition B' as a function of free-stream velocity.

	U (m/s)	R_M	R_d
○	3·05	163	24·5
□	3·81	204	30·6
■	4·57	245	36·8
▲	5·33	286	42·9
●	6·10	326	49·0

clues to the behaviour of the turbulence manipulators or to the mechanisms currently believed to be responsible for such behaviour.

Screens

Figure 4 (*a*) is a plot of the streamwise turbulence intensity u'/U_∞ versus downstream distance for screen 0 at different freestream velocities in flow condition B'. The turbulence intensity of the free stream for the test-flow condition is also shown for comparison. It is evident that, for free-stream velocities below 4·6 m/s, the turbulence intensity downstream of the screen remains below that of the free-stream condition. This is commonly known as the subcritical range (Schubauer *et al.* 1950), where the incoming turbulence is simply damped out by the screen. When U_∞ is increased beyond a threshold, in this case about 4·6 m/s, the character of the turbulence intensity profile begins to change. Immediately downstream of the screen the

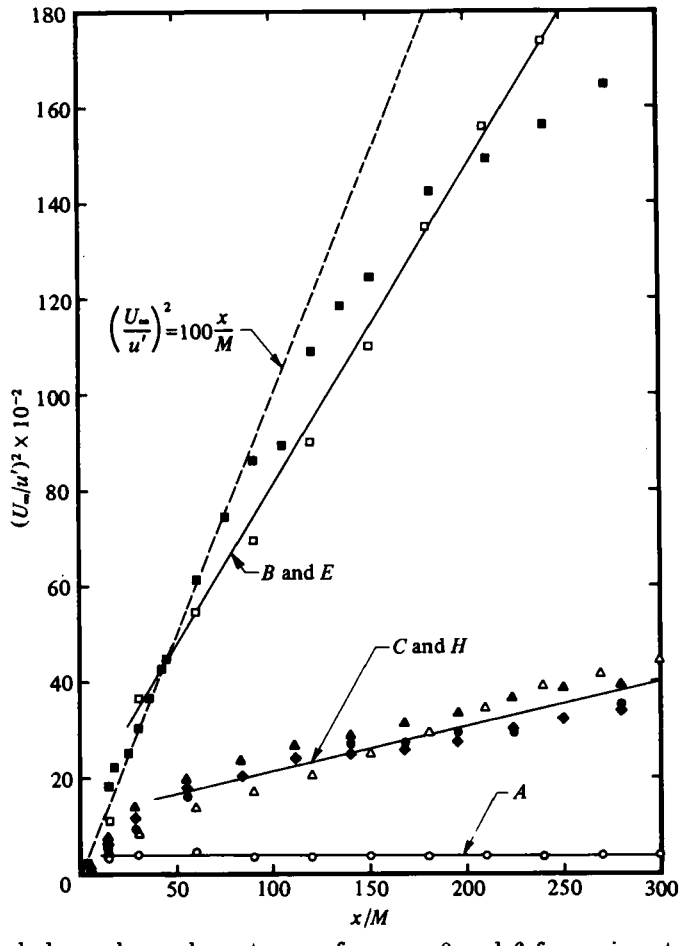

FIGURE 6. Turbulence decay downstream of screens 0 and 6 for various test-flow conditions. Screen 0 in flow condition: ○ *A*, □, *B*, △ *C*; with U_∞ = 4·6 m/s. Screen 6 in flow condition *H*: ● U_∞ = 7·6 m/s, ◆ 15·2 m/s, ▲ 22·9 m/s. ■ screen 6 in flow condition *E* with U_∞ = 15·2 m/s.

intensity rises rapidly to a peak above the free-stream condition and then decays further downstream, indicating that the screen is operating in the critical range, $R_d \simeq 40$. In this regime, small changes in U_∞ or the upstream disturbance level result in large changes in the character of the flow downstream of the turbulence manipulator. Increasing the free-stream velocity further increases the magnitude of the u'/U_∞ peak, although the axial position where this instability peak occurs remains unchanged. In the latter case, the screen is operating in what is commonly known as the supercritical range, i.e. $R_d > 50$. In all regimes, the intensity of turbulence far downstream of the screen, i.e. $x/M_{\text{screen}} > 200$, is lower than that of the test-flow condition. Spectra of the flow downstream of screen 0 in the same flow condition are presented in figure 4(*b*). At flow velocities below critical, the spectra reveal no significant peaks but, when the flow velocity is above critical, regular instability peaks can be seen at about 1·65 kHz and 1·72 kHz. The spectral peaks obtained close to the screen (i.e. at small x) are not unique in the sense that their relative magnitudes, and even the frequencies at which the peaks occur, depend on the location of the hot-wire sensor with respect to the mesh.

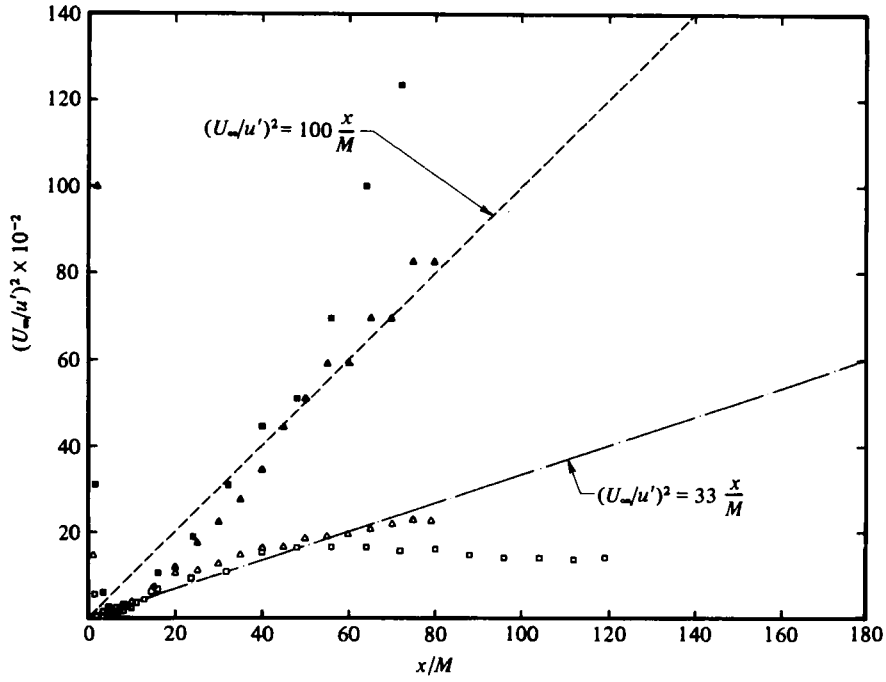

FIGURE 7. Effect of upstream flow on turbulence decay downstream of screens 3 and 5 for $U_\infty = 4{\cdot}6$ m/s. Open and solid symbols represent data taken in flow conditions A and B' respectively.

		Screen	R_d	R_M
□	■	3	83	460
△	▲	5	190	735

The data in figure 4(a) were replotted in figure 5 as $(U_\infty/u')^2$ versus a non-dimensional downstream distance. The lines $(U_\infty/u')^2 = 100x/M$ and $(U_\infty/u')^2 = 1000x/M$ are only intended to act as a guide for the reader. This figure demonstrates that for $x/M > 20$ the turbulence decay rate is highly sensitive to the free-stream velocity when the screen is operated subcritically. An increase in velocity decreases the turbulence decay rate in this regime. At $x/M \simeq 80$, the rate of decay is seen to decrease abruptly to a much smaller value. An abrupt change at the same x/M was also documented for $U_\infty = 3{\cdot}05$ m/s but the ordinate is not high enough in this reproduction of the figure to show it. The 'break' or discontinuity in the slope occurs farther downstream and is less pronounced at higher free-stream velocities. At $U_\infty = 5{\cdot}3$ m/s (above critical) it was difficult to detect a significant change in the slope of $(U_\infty/u')^2$ versus x/M for the range of downstream distances shown here.

In addition to the free-stream velocity, the turbulence decay rate downstream of screens can be affected by the level and structure of the incoming turbulence as shown in figure 6. The decay rates for screen 0 and screen 6 are presented in this figure for various test-flow conditions. The present data indicate that high turbulence decay rates are possible when the incoming turbulence intensity is relatively low and when the flow upstream of the screen contains no large-scale turbulence (compared to the screen mesh size) or swirls. Decay rates are appreciably lower in turbulent flows of moderate intensity such as the data obtained with screen 0 and screen 6 in

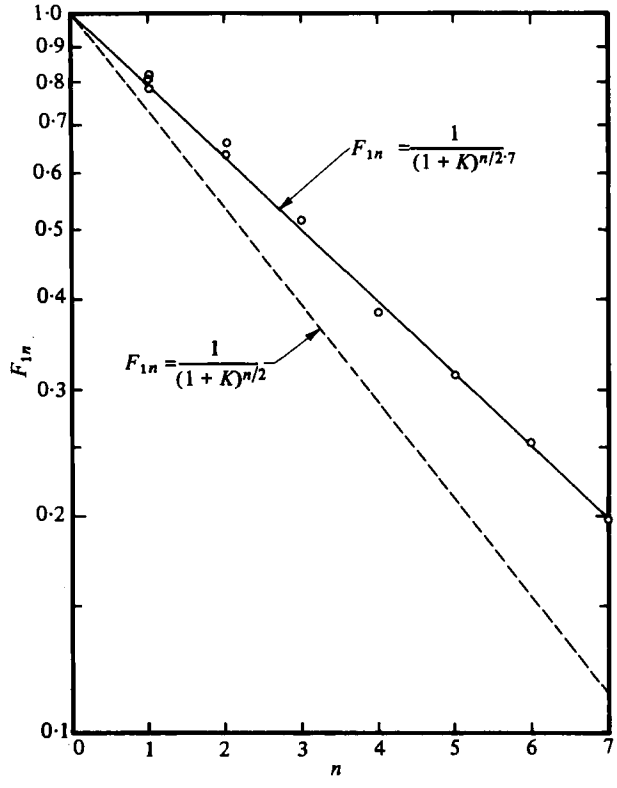

FIGURE 8. Turbulence-reduction factor versus number of screens in test-flow condition A, using screen 0.

test conditions C and H respectively. Finally, in an extreme (but not uncommon) case, the decay of turbulence downstream of a screen may be very slow when the incoming flow consists of large-scale turbulence and/or swirling motions and gross inhomogeneity of the mean flow, as suspected in test-flow condition A (Loehrke & Nagib 1972). In this case, a honeycomb can be used first to eliminate effectively the large-scale vorticity and swirling motions, as discussed by Wigeland *et al.* (1978). The effect of upstream turbulence conditions on the decay rates downstream of screens is further documented in figure 7 for screens 3 and 5 in flow conditions A and B'. Note that the decay rates diverge from each other and that screen 3 has the same solidity as 0 but twice the mesh and wire size, and hence operates at higher Reynolds numbers.

Figure 8 shows the streamwise turbulence-reduction factors (i.e. ratios of downstream to upstream turbulence intensity; for a complete definition see Loehrke & Nagib 1972) for a number of screens placed in series. Analyses and experiments by Dryden & Schubauer (1947) indicated that, for n screens placed in series, the streamwise turbulence-reduction factor is given by $F_{1n} = 1/(1+K)^{\frac{1}{2}n}$. In our experiments, conducted in flow condition A, the data did not fit Dryden & Schubauer's (1947) expression but rather the exponent was found to be $n/2{\cdot}7$. We conjecture that this discrepancy is a result of differences in test conditions between Dryden & Schubauer's (1947) case and ours. Their tests were probably conducted in a free stream with

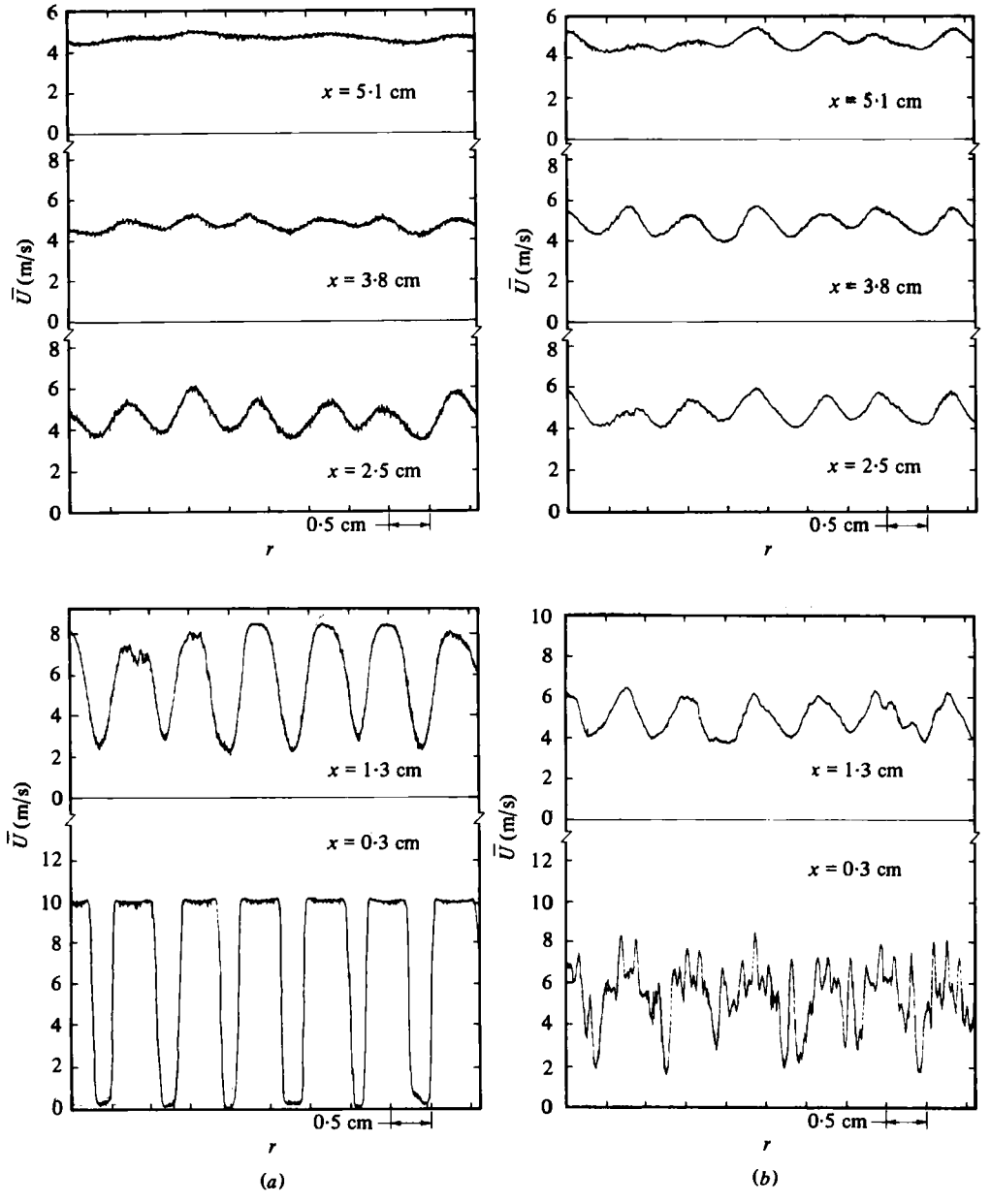

FIGURE 9. Transverse profiles of $\bar{U}$ for $U_\infty = 4{\cdot}6$ m/s and test-flow condition B: (a) downstream of PP3; (b) downstream of PP3/screen 0 combination with $\Delta x = 0$.

lower turbulence levels, without large-scale swirls which might have plagued flow condition A in the present investigation.

Perforated plates

Three perforated plates, PP1, PP2 and PP3, having high to medium solidities were used in the present investigation (see table 1 for their physical characteristics). All the perforated plates were operated in the supercritical regime. Figure 9(a) shows

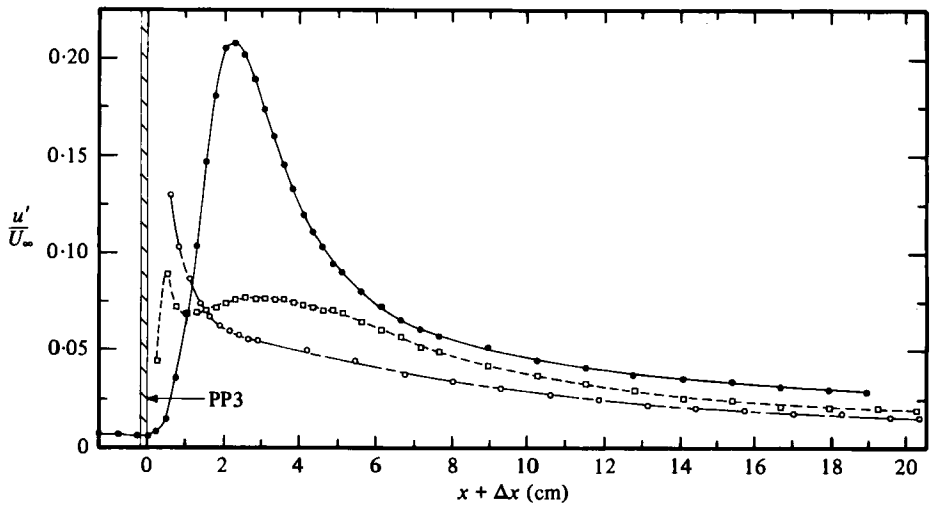

FIGURE 10. Streamwise development of turbulence intensity downstream of PP3 alone and in combination with screen 0, in test-flow condition B': ● no screen, □ $\Delta x = 0$, ○ $\Delta x = 0{\cdot}32$ cm.

radial profiles of $\overline{U}$ downstream of PP3 at increasing downstream distances in flow condition B. Sharply defined, jetlike profiles are found close to the perforated plate ($x = 0{\cdot}3$ cm). Further downstream, the mixing gradually smoothes out the non-uniformities in the mean velocity and by 5 cm downstream ($U_\infty = 4{\cdot}6$ m/s) there is no evidence of the jetlike character in the mean velocity $\overline{U}$ and the flow is fairly uniform. The development and decay of turbulence downstream of this grid is summarized in figure 10.

The spectra of u for PP3 in test conditions A and B are shown in figure 11 (a, b). The absence of high 'background' turbulence in condition B, particularly at the lower frequencies, reveals more of the structure of this plate-generated turbulence. In particular, this is demonstrated by observing the growth of the peak near 850 Hz between $x = 0{\cdot}51$ cm and $x = 1{\cdot}27$ cm, which is quite clear in figure 11 (b) (flow condition B) but is masked by the higher background turbulence of flow condition A (figure 11 a).

Perforated-plate/screen combinations

Figure 9 (b) depicts the transverse velocity profiles for the perforated plate PP3 in test-flow condition B but with screen 0 attached to its downstream side. By observing the data at increasing downstream distances, i.e. from the bottom of the figure upwards, one can see how the previously well-defined jets (figure 9 a) have been 'chopped up' by the addition of a screen, thereby introducing smaller scales into the flow. Small-scale turbulence is dissipated faster by the action of viscosity. However, this may not be beneficial as shown by the velocity record taken at $x = 5{\cdot}1$ cm. Substantial remnants of an undulating mean velocity profile indicate the presence of significant large-scale non-uniformities. Comparing figures 9 (a) and (b), it is evident that, by adding a 'chopper-screen' on the downstream side of PP3, the overall turbulent mixing has been partially suppressed, resulting in lower turbulence levels but a less uniform mean flow at similar downstream locations. This observation was further substantiated by examining the axial u'/U_∞ profiles shown in figure 10. The

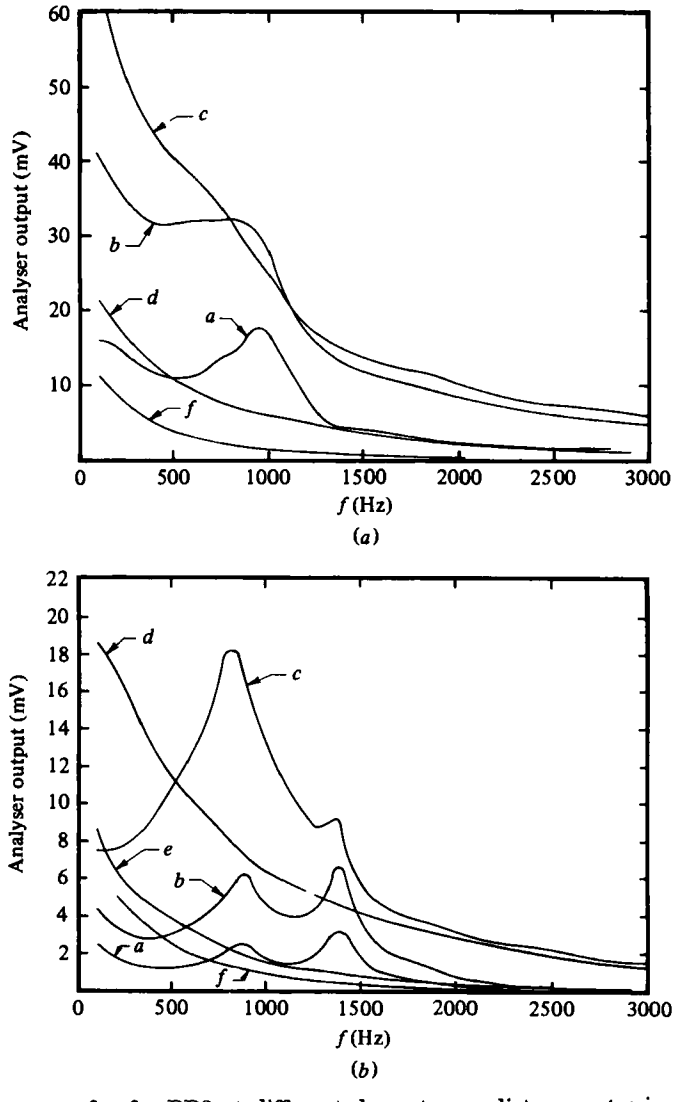

FIGURE 11. Spectra of u for PP3 at different downstream distances: (a) in test-flow condition A, (b) in test-flow condition B.

		(a)		(b)	
	x (cm)	$\bar{U}$ (m/s)	u' (mV)	$\bar{U}$ (m/s)	u' (mV)
a	0·5	9·8	165	9·8	30
b	0·8	7·7	400	9·4	62
c	1·3	5·9	515	8·1	165
d	5·1	4·5	145	4·8	155
e	15·2	—	—	4·8	55
f	25·4	4·9	70	4·9	40

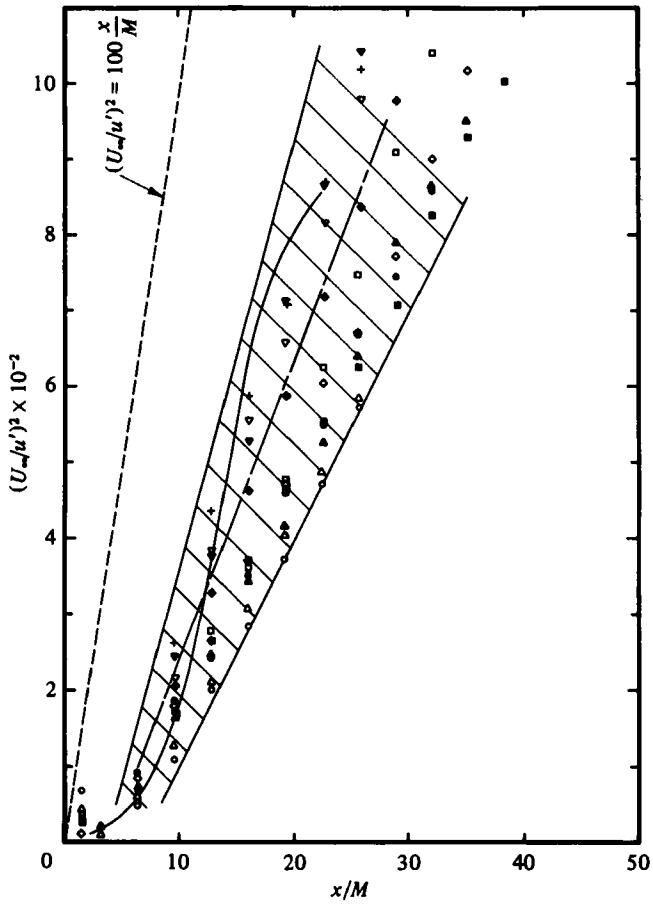

FIGURE 12. Turbulence decay downstream of PP3 in a variety of test-flow conditions and at different velocities. Test-flow condition A: ——— U_∞ = 4·6 m/s. Condition B: – — – 4·6 m/s. Condition E: ○ 7·6 m/s. Condition E': ◆ 4·6 m/s, ▽ 7·6 m/s, ▼ 15·2 m/s, + 23 m/s. Condition H: ◇ 4·6 m/s, ■ 7·6 m/s, □ 14·7 m/s, ▲ 15 m/s, △ 23 m/s. Condition $H1$: ●7·6 m/s.

holes of PP3 are sufficiently large so that the hot-wire probe could be brought in line with one of them and traversed upstream of the plate through the opening. The solid symbols show the turbulence intensity for PP3 without the downstream chopper-screen. During the acquisition of the data it was noted that the turbulence intensity dipped slightly as the sensor passed through the hole and then began a sharp rise to a high peak. After reaching what appears to be a saturation level, the turbulence intensity decays as the distance from the plate is increased. The open squares represent the turbulence intensity profile corresponding to the situation in figure 9 (*b*) with a screen attached downstream of the grid and no separation distance between them, i.e. $\Delta x = 0$. In this case the characteristic peak in u'/U_∞ a short distance downstream has been suppressed by the addition of the screen. Except for very close to the manipulator, the turbulence intensity is everywhere lower with the screen than without it. By adding a separation distance between the perforated plate and the screen, the turbulence intensity is further reduced. This is demonstrated in figure 10 by data for Δx = 0·32 cm, i.e. $\Delta x/M_{\mathrm{PP}} = 0{\cdot}4$.

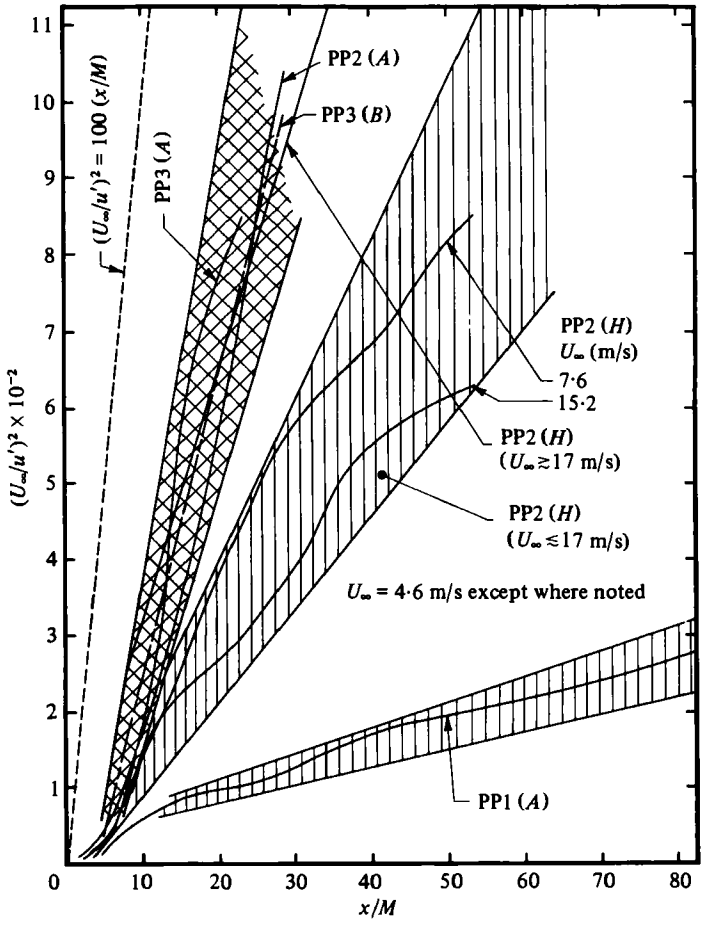

FIGURE 13. Turbulence decay downstream of PP1, 2, 3 under different test-flow conditions.

Figure 12 presents the decay of turbulence for PP3 under a variety of test-flow conditions and at different free-stream velocities. The data from this perforated plate, $\sigma = 0{\cdot}42$, indicate that for operation in the supercritical regime, i.e. in presence of significant turbulence generation by the flow manipulators, the turbulence decay rate is relatively insensitive to upstream flow conditions, including the flow velocity, turbulence intensity and scales.

The turbulence decay rate is shown versus a non-dimensional downstream distance for the different perforated plates in a variety of test-flow conditions and free-stream velocities in figure 13. It is interesting to note that the large volume of data fell roughly within the shaded bands. The cross-hatched band corresponds approximately to the one shown in figure 12. This band represents not only all of the data from the 'moderate-solidity' PP3, but also the turbulence decay data for the 'moderately-high-solidity' PP2 ($\sigma = 0{\cdot}49$) when the free-stream velocity exceeds approximately 17 m/s. The rate of turbulence decay downstream of PP2 in flow condition *H* was found by Ahmed *et al.* (1976) and by Fraissenet (1976) to be dependent on the flow velocity. As summarized by figure 13, the turbulence seems to decay much more

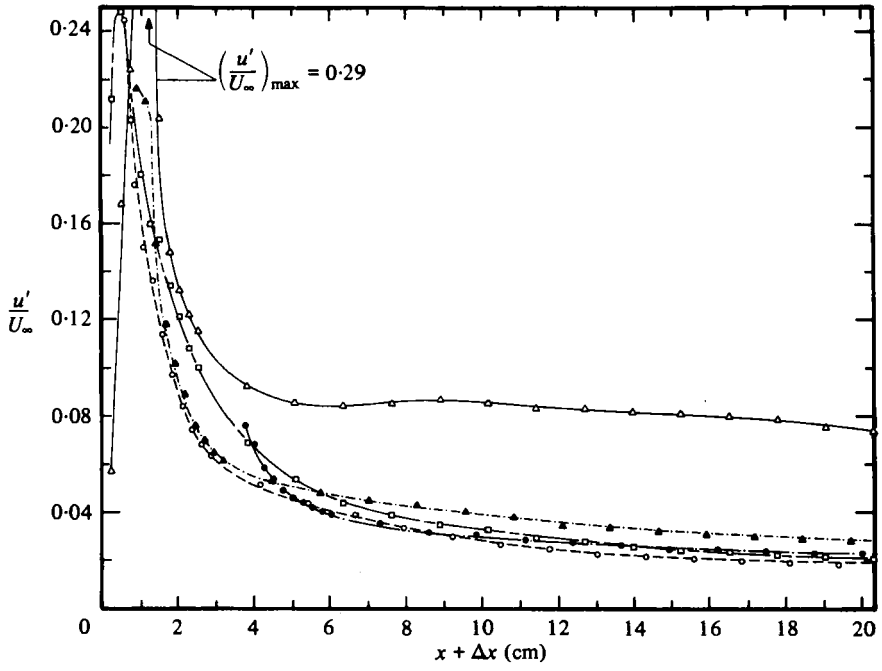

FIGURE 14. Streamwise development of turbulence intensity in test-flow condition *A* downstream of PP1, alone and in combination with screen 0. △ no screen, □ $\Delta x = 0$, ○ 0·32 cm, ▲ 0·64 cm, ● 3·49 cm.

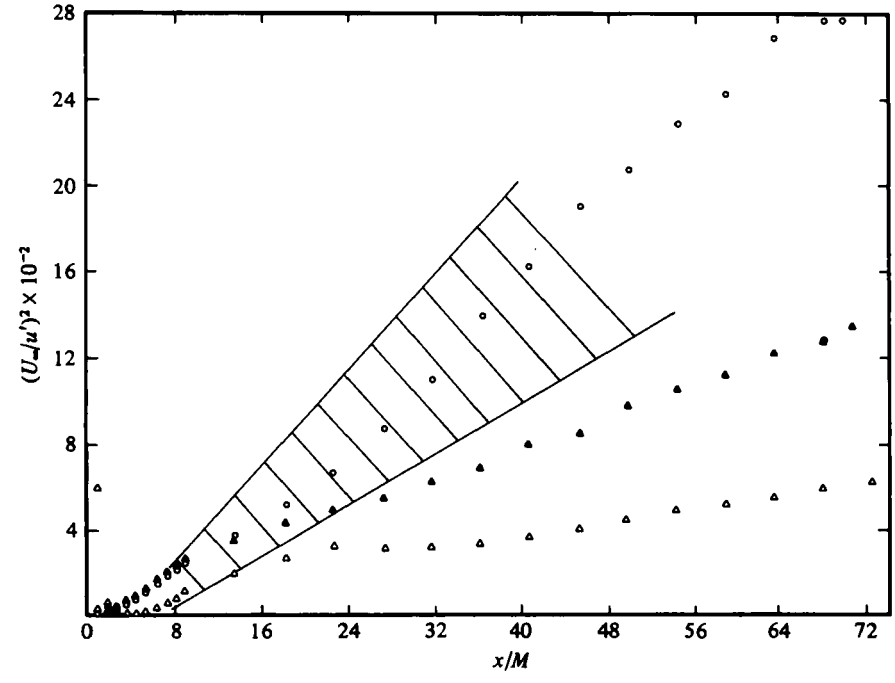

FIGURE 15. Turbulence decay in test-flow condition *A* downstream of PP1, alone and in combination with screen 0, and downstream of PP3. Shaded region PP3; △ PP1/no screen, ○ PP1/screen with $\Delta x = 0{\cdot}32$ cm, ▲ PP1/screen with $\Delta x = 0{\cdot}64$ cm.

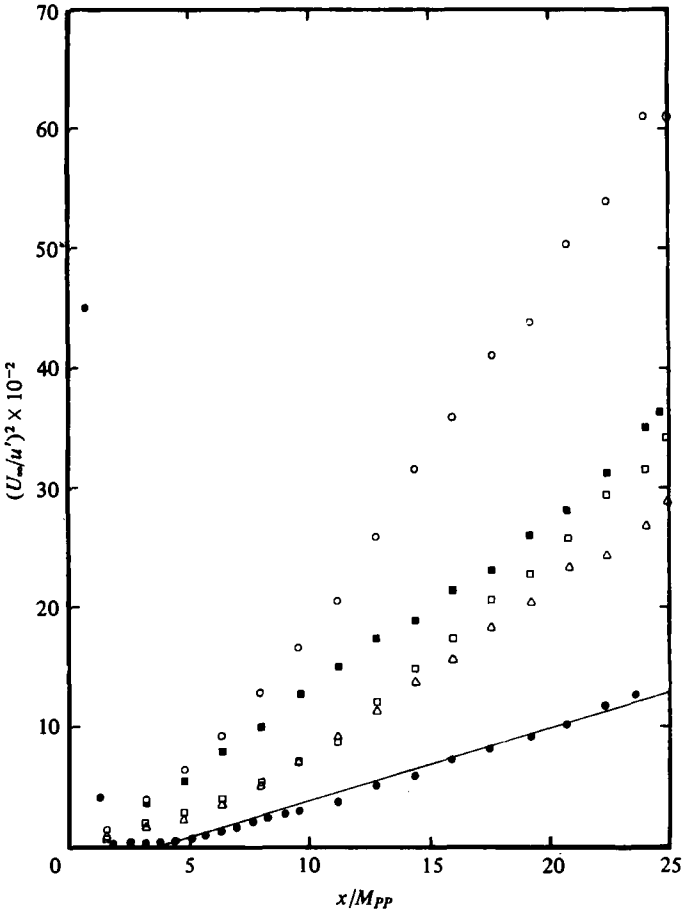

FIGURE 16. Effect of separation distance Δx on turbulence decay downstream of PP3/screen 3 combination in test-flow condition B', with M_{PP} = 0·80 cm: ● no screen, □ Δx = 0, ○ 0·32 cm, ■ 0·64 cm, △ 0·95 cm.

slowly if the velocity is below 17 m/s and if the upstream flow is free from large-scale motions and has a low turbulence level.

The band having the lowest decay rate in figure 13 encompasses the data for the high-solidity (σ = 0·7) PP1 in flow condition A. Visualization records (see figure 75(a) of Loehrke & Nagib 1972) have demonstrated that the irregular behaviour of this high-solidity plate is probably due to the bunching up of individual jets into separate groups, each composed of several jets, and the existence of some reversed flow. We have adopted the designation 'anomalous behaviour' as a description of the character of turbulence downstream of such high-solidity manipulators. However, since high-solidity perforated plates or grids may find application in flow management where a high pressure drop is required, attempts were made to see if the turbulence decay performance could be improved by the addition of a screen downstream of them. Corrsin (1944) had some success utilizing this idea in a similar situation.

Figure 14 demonstrates that the turbulence intensity profile downstream of the

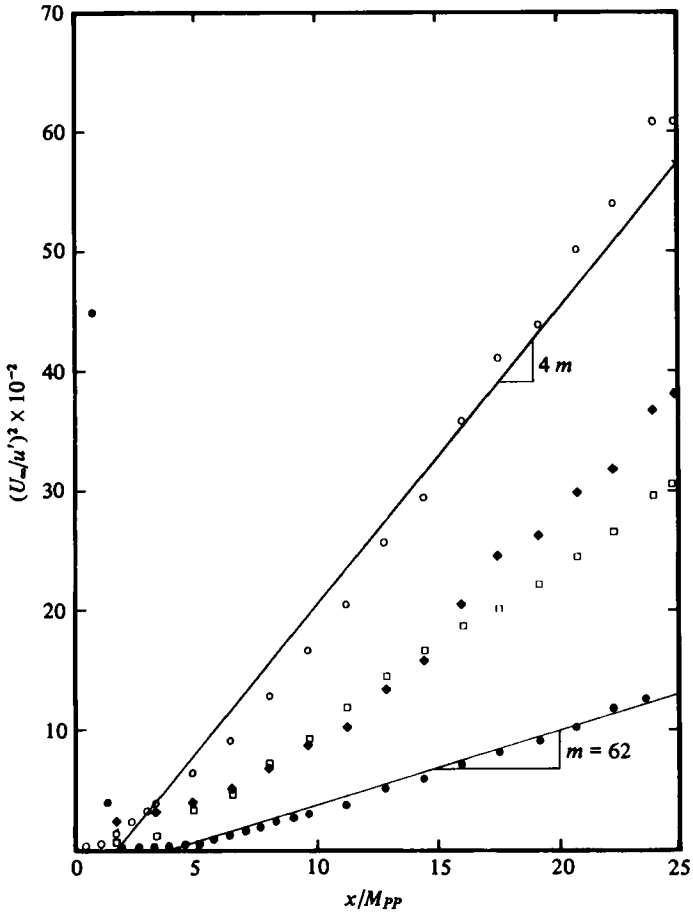

FIGURE 17. Effect of scale-matching on turbulence decay in test-flow condition B' downstream of PP3 in combination with: ● no screen; ◆ screen 0 at Δx = 0·32 cm (M_{PP}/M_{screen} = 9·5), ○ screen 3 at 0·32 cm (M_{PP}/M_{screen} = 5·0), □ screen 5 at 0·64 cm (M_{PP}/M_{screen} = 3·2).

high-solidity PP1 can be made comparable to that of moderate-solidity grids (cf. figure 10) by the addition of a screen downstream of the plate, but only when the separation between the manipulators has been optimized. Data not shown here (Tan-atichat *et al.* 1972) indicate that the optimum separation depends on the characteristics of the screen, and in particular on the pressure drop across it. The data of figure 14 are replotted in figure 15 as turbulence decay curves to illustrate further the tremendous improvement in the rate of decay in the presence of an 'optimum screen' placed at the optimum separation, as well as to compare it with the performance of the moderate-solidity grid PP3 and the anomalous behaviour of PP1 without a screen.

Results from a combination of PP3 with screen 3 demonstrate that other plate–screen combinations also produce improved turbulence decay rates, such as in the case of 'moderate-solidity' plates, as shown in figure 16. The effect of changing the intermanipulator separation is clearly demonstrated by an increase in the decay rate as Δx is changed from 0 to 0·32 cm. With further increases in the intermanipulator

separation, a drop in the turbulence decay rate is noted. Clearly there is an optimum separation distance for maximum turbulence decay. Other combinations were tried with similar results but are not presented here due to space limitations. By plotting the data as turbulence decay versus a non-dimensional downstream distance, several PP3 and screen combinations were compared for the best turbulence decay in test-flow condition B', as shown in figure 17. The data obtained using PP3 alone is included as a reference. Close examination of figure 17 reveals that the turbulence decay rate of the combination could be increased to four times that of the plate alone when the proper screen and intermanipulator distance are chosen. The mesh ratio between PP3 and the optimum screen, $(M_{\mathrm{PP}}/M_{\mathrm{screen}})$, was found to be about 5. Higher or lower ratios produced slower turbulence decay. The combination of PP3 and screen 3 with an intermanipulator distance of 0·32 cm, i.e. $\Delta x/M_{\mathrm{PP}} = 0{\cdot}4$, was found to produce the fastest turbulence decay rate when compared to all combinations of the plate with the other screens. It is therefore very important to match turbulence manipulators when they are going to be used in a closely coupled combination.

4. Discussion

This section aims to summarize the main findings of this paper by discussing all of the results from the previous sections. In order to do this, the general definition of a turbulence manipulator given by Loehrke & Nagib (1972, 1976) is adopted. A turbulence manipulator can be thought of as an operator which transforms the incoming turbulence into exiting turbulence of different intensity and structure. For present purposes, the incoming flow characteristics will be defined as those which would exist at the locus of the leading edge of the device in the absence of the device. The downstream boundary of the device is considered (operationally) to be located where the streamwise gradients of the mean and fluctuating velocities, $\partial U/\partial x$ and $\partial u'/\partial x$, are about the same as they would be in the absence of the device. Because of the similar geometry of all the manipulators discussed here, we differentiate between them (i.e. classify them) only on the basis of their solidity or their characteristic Reynolds numbers.

Shear-layer instability and manipulator performance in subcritical, critical and supercritical regimes

The effectiveness of manipulators in achieving a net reduction in turbulence depends not only on the ability of the device to quench incoming turbulence, but also on the generation of new turbulence with the appropriate scales. These scales must be smaller than the corresponding ones in the incoming flow, but should not be much smaller, to allow for the spectral transfer of energy towards the dissipative scales. The appropriate matching of scales leads to enhanced decay of the turbulence energy downstream of the manipulator. The new turbulence is a result of the shear-layer instability produced by the wake of the manipulator: hence its scales can be controlled by appropriate design of the device. For subcritical operation there is little or no growth in the instability, and turbulence far downstream of the device decays approximately at the original rate, as is the case of screens in low velocities (e.g. figures 4 and 5; $x/M \gtrsim 80$). However, the initial decay of turbulence is governed by the damping characteristics of the screen, and hence is very dependent on the free-

stream velocity, as demonstrated in figure 5. In view of this and earlier observations, screens should not be operated in the subcritical or critical regime, particularly when the turbulence reduction is to be independent of free-stream velocity. Unfortunately, this is a very likely condition that exists in the settling chambers of some wind tunnels.

Operation in the critical regime can cause the performance to change abruptly with small changes in the free-stream velocity or upstream turbulence (e.g. room conditions in open-return wind tunnels and test-object or fan conditions in closed-return tunnels). Detailed measurements downstream of above-critical and below-critical screens can be found in the classical work of Schubauer *et al.* (1950) (see their figures 5 and 6). In figure 13 of their report, the empirical critical Reynolds number of the screen (based on wire diameter and free-stream velocity) is plotted as a function of the screen solidity.

A total of seven screens were used in the course of the present investigation. According to figure 13 of Schubauer *et al.* (1950), at a free-stream velocity of 4·6 m/s three of the screens are below-critical, three are above-critical and one is just subcritical. Moderate instability peaks were observed in the axial development of u' downstream of the subcritical screens when the incoming flow was the highly disturbed condition A. Even the milder disturbances of condition B generally caused these peaks and the tell-tale spectral growth in discrete high frequencies. For example, in figure 4 the screen operated in the subcritical regime according to Schubauer *et al.* (1950); $R_d = 40$, $\sigma = 0{\cdot}28$. However, some spectral growth near 1400 Hz is observed at 7·5 mesh lengths downstream of the screen, i.e. near the instability peak of figure 4 (a). This spectral excitation appears consistent with subcritical instabilities downstream of a cylinder in uniform flow in the presence of finite disturbances. These observations should be compared with the remarks on p. 15 of Schubauer *et al.* (1950): '. . . critical Reynolds numbers were unchanged when the incident turbulence was raised . . .'. It was suspected that the difference between the turbulence of Schubauer *et al.* (1950), u'/U_∞ of 0·7 % for the precritical cases, and 1·5 % and 8 % for conditions B and A respectively, might account for the difference in observations. Special conditions were engineered with u'/U_∞ of 0·7 % and 0·2 %. The corresponding sudden onset of regular fluctuations immediately downstream of the screen occurred at 4·9 and 6·1 m/s. Thus, contrary to the conclusion of Schubauer *et al.* (1950), subcritical instabilities indeed appear to depend on the level of the finite disturbances.

The behaviour of PP2 in test-flow condition H (figure 13) clearly shows an abrupt change in the turbulence decay rate when the free-stream velocity is increased beyond 17 m/s. Although we do not know the exact details of the mechanisms responsible for this peculiar behaviour, we conjecture that they are related to an instability threshold. In this case, the instability may be associated with the coalescing of the jets from the holes of this 'moderately-high-solidity' grid, i.e. anomalous behaviour. As a result, it is recommended that high- and moderately-high-solidity devices be avoided. However, the lower the operating Reynolds number, the lower will be the 'safe' upper limit of the solidity range. Therefore, for grids a solidity of 0·4 appears to be a safe maximum, while for screens $\sigma = 0{\cdot}3$ may be as high as one should use in important applications.

At high enough Reynolds numbers, the flow through turbulence manipulators exhibits strong shear-layer instabilities that grow rapidly until nonlinear mechanisms

take over and turbulence results. Spectral analysis (figures 4(*b*) and 11) shows that these are distinct peaks in frequency. Although the rate of turbulence decay is lower in this regime, it is relatively independent of the free-stream velocity, as shown in figure 6 for screen 6 in test-flow condition *H*. Perforated plate 3 also exhibits a turbulence decay rate which is not only independent of velocity, but also insensitive to the upstream flow conditions, as shown in figure 12. This insensitivity to upstream conditions is brought about by the effective damping module of the higher-solidity grid and the very large amount of turbulence generated by the device. Both of these effects tend to overwhelm the upstream condition. The decay rate for the grid in figure 12 changes at larger downstream distance as the turbulence approaches the final period of decay, as demonstrated in figures 5 and 6 for screens.

Influence of upstream turbulence on performance of turbulence manipulators

Another very important point to keep in mind in selecting a system for turbulence reduction is the fact that the performance of turbulence manipulators may not be identical for all incoming flow-field structures. The structure of the incoming flow may be characterized by the level of turbulence, its macroscale, the spatial distribution of the mean and fluctuating velocity components, and the spectral distribution of the energy of the fluctuating velocity components (e.g. Loehrke & Nagib 1972; Tsuji 1955, 1956). Figure 6 shows that, in low-turbulence test-flow conditions *B* and *E*, the turbulence decay rate downstream of screens is highest, while in moderate turbulence levels (conditions *C* and *H*) the decay rate is lower. The turbulence decay rates downstream of supercritically operated screens for both the low and moderate turbulence levels are relatively independent of the free-stream velocity. However, when there is swirl or other large-scale inhomogeneities in the flow, screens cannot perform well in turbulence reduction as shown for the case of screen 0 in test-flow condition *A* at the bottom of figure 6. Further evidence of decay-rate dependence on turbulence structure is shown in figure 7 for screens 3 and 5. Both screens have higher decay rates in the low-turbulence condition *B'* as compared to the decay rates in test-flow condition *A*. It is conjectured that the behaviour observed in figures 6 and 7 is a consequence of the influence of upstream turbulence on the 'combined' downstream decay rate. Therefore, the initial period of decay of screen-produced turbulence is easier to discern when the background turbulence level is low.

The turbulence reduction factor F_{1n} for n screens placed in series, which was measured in condition *A*, proved to be consistently different from the results of the controlled experiments of Dryden & Schubauer (1947). The present data, summarized in figure 8, correlate well according to $F_{1n} = 1/(1+K)^{n/2\cdot7}$. Comparison with $F_{1n} = 1/(1+K)^{\frac{1}{2}n}$ of Dryden & Schubauer (1947) again hints at the decreased effectiveness of screens in the adverse condition *A*. In such conditions one may require an extra screen, with the concomitant increase in pressure drop, to accomplish the desired reduction in free-stream turbulence.

Differences in the spectra of u downstream of a grid at various axial positions for flow conditions *A* and *B* are evident from figure 11. The instability peaks which occur at nearly discrete frequencies are more prominent in the low-turbulence condition *B*. In this low-turbulence condition we can trace the evolution of the two spectral peaks as we progress downstream. Initially, a peak appears at the instability frequency $f_i^* = 1400$ Hz and further downstream it is at a lower frequency, $f^* = \frac{3}{5}f_i^*$

(= 850 Hz). As the downstream distance is further increased, the peak at f^* dominates. Both f^* and f_i^* are linearly proportional to U_∞ and thus are presumably associated with inviscid instabilities and fixed characteristic scales (see section *B* of Results in Nagib *et al.* 1975, p. 512).

The important role of the shear-layer instability has been established and discussed in detail in the previous sections. The observed trends indicate strong effects of upstream turbulence, not only on the generation of new turbulence through remnant Reynolds stresses, but also on the development and evolution of the shear-layer instabilities. As discussed in the previous section, the turbulence decay rate of perforated plate 2 shown in figure 13 is also quite dependent on the upstream turbulence condition, as well as being a function of the Reynolds number.

Anomalous performance of high-solidity turbulence manipulators

The flow downstream from PP1 exhibits characteristics that are not common to the other two grids. In particular, certain irregularities in the mean velocity profile (e.g. see figure 30 of Loehrke & Nagib 1972) develop and persist far downstream. Also, the decay of u'/U_∞ downstream from PP1 (open triangles on figure 14) is much slower than that of the other two grids. This behaviour is emphasized in figure 13, where the turbulence decay, plotted as $(U_\infty/u')^2$ versus x/M, for PP1 is grossly lower than that for PP2 and PP3. The most plausible explanation for this disparity lies in the interaction and coalescing of the jets issuing from high-solidity grids, screens and multiple jets noted by Corrsin (1944), Klebanoff & Tidstrom (1959), Bradshaw (1965) and Schubauer *et al.* (1950) (see Corrsin 1963, §A-6). This explanation is supported by the hydrogen-bubble visualization of the flow immediately downstream from PP1 in figure 75(*a*) of Loehrke & Nagib (1972).

The lateral velocity gradients associated with the non-uniformities in the mean velocity profile persist for large downstream distances and contribute to the production of turbulence downstream of high-solidity grids through the terms $\overline{uv}\,\partial U/\partial y$ of the turbulence energy equations. In spite of the general decay of turbulence, it appears that in these cases sufficient Reynolds stresses remain at large x/M and participate in this production mechanism, leading to slower net rates of turbulence decay. Successful techniques to remedy this 'anomalous' behaviour must therefore rely on the early elimination of the non-uniformities in the mean velocity or on preventing their formation.

Improvements in performance of grids by combining them with screens

A series of experiments was performed to investigate the effect of a passive device, namely screen 0, on this anomalous behaviour. The screen was placed downstream of PP1 at several separation distances. An intermanipulator separation of $\Delta x/M_{\mathrm{PP}} = 0{\cdot}8$ produced a decay rate of about 16·9 based on x/M while a separation of $\Delta x/M_{\mathrm{PP}} = 0{\cdot}4$ improved the decay rate by a factor of almost three to 48·8. This combination is comparable in performance to non-anomalous grids. It is believed that the added screen generates smaller-scale turbulence which prevents the coalescing of the individual jets that would have spawned larger and more coherent eddies. If the larger eddies are formed, the added small-scale turbulence aids in dissipating them. In addition, some visualization experiments in water have indicated that the

presence of the screen near optimum separation tends to stabilize the unsteady coalescing and to inhibit the formation of gross non-uniformities to some extent. We conjecture that the pressure drop provided by the screen is partially responsible for this. The large reduction of turbulence achieved by a tandem screen opens up the prospect of curing the anomaly of wind tunnels in which 'high-solidity' devices have been inadvertently or intentionally installed to achieve a large pressure drop in a short streamwise distance (with corresponding adverse effects on turbulence intensity and uniformity).

The substantial improvement in the performance of PP3 by the addition of a chopper screen has been demonstrated in figures 16 and 17. With screen 3 placed downstream of the plate, the turbulence decay rate increases significantly. When a small separation distance is provided between the grid and screen, the decay rate is higher still. However, with further increases in the separation distance, the decay rate drops. Clearly there is an optimum separation distance where the decay rate is highest. Therefore, one parameter which plays a key role in the performance of combined manipulators is the intermanipulator separation Δx. As pointed out in the previous paragraph, this optimization process relies partly on the proper matching of the turbulence scales between the two coupled manipulators, and partly on the pressure drop of the downstream one.

Another important parameter to consider when using combined manipulators that are closely coupled is their mesh ratios, i.e. $M_{\mathrm{PP}}/M_{\mathrm{screen}}$. Different grid and screen combinations have been tried by utilizing three screens having different mesh sizes with the same perforated plate at various separation distances. The mesh ratio in the above test ranged from about 3 to 10. The turbulence decay rates for these combinations are summarized in figure 17. In all of the above cases, there is a definite improvement in the decay rate for the 'combined manipulator' over the grid alone. However, the highest decay rate is achieved with an intermediate mesh ratio of about 5. For all combinations shown, the results have already been chosen from the optimum plate-to-screen separation distance. If we refer the decay rate to that of a perforated plate alone, the present results indicate that it is possible to obtain a turbulence decay rate 4 times higher by choosing the proper scaling between the grid and screen and by optimizing the separation distance between them. While the complete spectral documentation has not been obtained for the flow downstream of the various combinations summarized in figure 17, it is conjectured that the optimum matching between the grid and the screen depends on the ratio between the scales of turbulence generated by them. This wavenumber ratio needs to be sufficiently large (> 3) to induce spectral transfer, but small enough (< 10) to prevent the formation of a large spectral gap between the turbulence scales. Loehrke & Nagib (1976) stated that 'an important, but not yet understood, relation must exist between the scales of the interacting shear layers of manipulators in series'. It is our hope that the present experiments have contributed to the understanding of this relation.

5. Conclusions

Shear-layer instabilities in the wake of screens and grids, and Reynolds stresses acting on the velocity gradients of the wake, are two key mechanisms responsible for generation of new turbulence downstream of these 'turbulence manipulators'.

The effectiveness of such passive devices in reducing free-stream turbulence depends on the balance between the generation of this new turbulence and the initial suppression of upstream turbulence by the manipulator. Careful matching of scales of the new turbulence to those of the upstream flow (after passing through the device) can lead to enhanced turbulence decay and to more effective net reduction in the free-stream turbulence; see the previous paragraph for guidelines for the matching of scales.

The performance of a turbulence manipulator, such as a screen or grid, is influenced by the structure of the upstream flow, including any swirls, large vortical motions or velocity non-uniformities, and the intensity and scales of the turbulence. The lower the solidity and Reynolds numbers of the device, the stronger the dependence. Therefore, published turbulence-reduction factors should not be generalized to all applications, especially where the turbulence to be controlled is different from that used in the original tests; this is particularly true in the case of screens.

Screens should not be operated in subcritical- or critical-Reynolds-number regimes, $R_d < 50$, particularly when turbulence reduction is to be independent of the free-stream velocity.

We recommend that high- and moderately-high-solidity manipulators be avoided due to the anomalous behaviour of the flow resulting from them; $\sigma = 0{\cdot}4$ and $0{\cdot}3$ is the maximum solidity advisable for grids and screens, respectively.

When high-solidity grids must be used, it is possible to improve the quality of flow downstream of them, as well as to increase the rate of turbulence decay, by placing a screen with a smaller pressure drop at an optimum separation downstream of the grid; $x/M \simeq 0{\cdot}5$.

The rate of turbulence decay downstream of all grids may be increased by as much as four times. The addition of a screen downstream of the grid at an optimum separation, $x/M \simeq 0{\cdot}5$, can lead to such improvements. The ratio of the mesh of the grid to that of the screen must be carefully selected so that the ratio of characteristic wavenumbers between grid- and screen-generated turbulence is large enough to induce spectral transfer ($M_{\text{grid}}/M_{\text{screen}} > 3$), but sufficiently small to prevent the formation of a substantial spectral gap between the two characteristic scales ($M_{\text{grid}}/M_{\text{screen}} < 10$).

REFERENCES

Ahmed, M., Wigeland, R. A. & Nagib, H. M. 1976 *Ill. Inst. Tech. Fluids & Heat Transfer Rep.* no. R76-2; *NTIS* no. AD-029 418.

Batchelor, G. K. 1945 *A.C.A. Rep.* no. 13.

Batchelor, G. K. 1953 *The Theory of Homogeneous Turbulence*. Cambridge University Press.

Bradshaw, P. 1965 *J. Fluid Mech.* **22**, 679–687.

Comte-Bellot, G. & Corrsin, S. 1966 *J. Fluid Mech.* **25**, 657–687.

Corrsin, S. 1944 *N.A.C.A. ACR* No. 4H24.

Corrsin, S. 1963 *Handbuch der Physik*, vol. 8, pp. 524–590.

Dryden, H. L. & Schubauer, G. B. 1947 *J. Aero. Sci.* **14**, 221–228.

Dryden, H. L. & Schubauer, G. B. 1949 Appendix to Taylor & Batchelor *Quart. J. Mech. Appl. Math.* **2**, 26–29.

Fraissenet, A. 1976 *Ill. Inst. Tech. Internal Rep.*

Hinze, J. O. 1975 *Turbulence*. McGraw-Hill.

KLEBANOFF, P. S. & TIDSTROM, K. D. 1959 *N.A.S.A. Tech. Note* no. D-195.

LAWS, E. M. & LIVESEY, J. L. 1978 *Ann. Rev. Fluid Mech.* **10**, 247–266.

LOEHRKE, R. I. & NAGIB, H. M. 1972 *AGARD Rep.* R-598.

LOEHRKE, R. I. & NAGIB, H. M. 1976 *Trans. A.S.M.E.* I, *J. Fluids Engng* **98**, 342–353.

NAGIB, H. M., WAY, J. L. & TAN-ATICHAT, J. 1975 *Prog. Astro. Aero.* **37**, 503–520.

SCHUBAUER, G. B., SPANGENBERG, W. G. & KLEBANOFF, P. S. 1950 *N.A.C.A. Tech. Note* no. 2001.

TAN-ATICHAT, J., NAGIB, H. M. & LOEHRKE, R. I. 1972 *Bull. Am. Phys. Soc.* **17**, 1097.

TAYLOR, G. I. & BATCHELOR, G. K. 1949 *Quart. J. Mech. Appl. Math.* **2**, 1–29.

TOWNSEND, A. A. 1976 *The Structure of Turbulent Shear Flow.* Cambridge University Press.

TSUJI, H. 1955 *J. Phys. Soc. Japan* **10**, 578–586.

TSUJI, H. 1956 *J. Phys. Soc. Japan* **11**, 1096–1104.

WIGELAND, R. A., AHMED, M. & NAGIB, H. M. 1978 *A.I.A.A. J.* **16**, 1125–1131.